Acta Mech 229, 5013–5029 (2018)
https://doi.org/10.1007/s00707-018-2286-0

ORIGINAL PAPER

Reza Bahaadini · Ali Reza Saidi · Mohammad Hosseini

Dynamic stability of fluid-conveying thin-walled rotating pipes reinforced with functionally graded carbon nanotubes

Received: 16 October 2017 / Revised: 7 September 2018 / Published online: 24 October 2018

Abstract In this study, vibration and dynamic stability of fluid-conveying thin-walled rotating pipes reinforced with functionally graded carbon nanotubes are studied. The pipe is modeled based on thin-walled Timoshenko beam theory and reinforced by single-walled carbon nanotubes with uniform distribution as well as three types of functionally graded distribution patterns. The governing equations of motion and the associated boundary conditions are derived via Hamilton's principle. The governing equations of motion are discretized via the Galerkin method, and the eigenfrequency and the stability region of the pipe are found using the eigenvalue analysis. Some numerical examples are presented to study the effects of length–radius ratio, carbon nanotubes distribution, volume fraction of carbon nanotubes, rotational speed and mass ratio on the non-dimensional eigenfrequency and critical flutter velocity of the thin-walled rotating pipe conveying fluid. The results show that the carbon nanotubes distribution has a significant effect on the non-dimensional eigenfrequency and critical flutter velocity. Also, it is found that the rotational speed has a stabilizing effect on the dynamic behavior of the system.

Keywords Dynamic stability · Thin-walled rotating pipe · Reinforced · Functionally graded carbon nanotube

1 Introduction

Recently, nanocomposite materials reinforced with carbon nanotubes (CNTs) have received a great deal of attention in numerous fields of science and engineering due to their unique properties [1]. Hence, the introduction of CNTs into polymeric composites may improve their applications in the fields of reinforcing composites, electronic devices and so on. Based on superior properties of functionally graded carbon nanotube-reinforced composites (FG-CNTRCs), mechanical analysis of the FG structures reinforced with CNTs has attracted much attention from researchers. For example, Ke et al. [2] studied the effects of CNT volume fraction, distribution pattern of CNTs, vibration amplitude and slenderness ratio on nonlinear vibration of FG-CNTRC beams. Based on the Timoshenko beam reinforced with CNTs, the vibration analysis and buckling analysis of nanocomposite beams resting on an elastic foundation were investigated by Yas and Samadi [3]. They examined the influences of nanotube volume fraction, slenderness ratios, CNT distribution, elastic foundation and boundary conditions on the natural frequency and critical buckling load. Yas and Heshmati [4] investigated the free and forced vibration of the nanocomposite beams reinforced by CNTs and subjected to moving load. Rafiee et al. [5]

R. Bahaadini · A. R. Saidi (✉)
Department of Mechanical Engineering, Shahid Bahonar University of Kerman, Kerman, Iran
E-mail: saidi@uk.ac.ir
Tel.: +98-34-32111763

M. Hosseini
Department of Mechanical Engineering, Sirjan University of Technology, Sirjan, Iran

studied the influences of nanotube volume fraction, CNT distribution, applied voltage, temperature change and beam geometry on linear and nonlinear frequencies of the FG-CNTRC beams with piezoelectric layers. Lin and Xiang [6] performed vibration of beams reinforced with CNTs based on both first-order and third-order beam theories. The bending, buckling and vibration of CNTRC beams resting on an elastic Pasternak foundation were investigated by Wattanasakulpong and Ungbhakorn [7]. The effects of nanotube volume fraction, CNT distribution, aspect ratio and in-plane forces on the flutter and divergence boundaries of the FG-CNTRC plates under a supersonic flow were analyzed by Fazelzadeh et al. [8]. The flow-induced instabilities of the FG-CNTRC panels in the supersonic flow and thermal environments were studied by Asadi et al. [9]. Lots of research works studied the mechanical characteristics of CNTRC structures (see, e.g., Alibeigloo and Liew [10], Mirzaei and Kiani [11] and Thomas and Roy [12]).

Pipes conveying fluid are fundamental dynamical issues in the field of fluid–structure interaction (FSI) and basic elements which are widely used in mechanical engineering, civil engineering, off-shore oil and gas industries and so on. The vibration analysis of the pipe conveying fluid is a common study in engineering problems, and knowledge of the fluid velocities proposes the designer avoiding the critical velocities. Vibration and dynamic instability of the pipes conveying fluid have been studied by Païdoussis [13], Kuiper et al. [14], Ghorbanpour Arani et al. [15], Hosseini and Bahaadini [16], Ning et al. [17], Kjolsing and Todd [18], Wang et al. [19], Bahaadini et al. [20–22], Hosseini et al. [23,24] and Askarian et al. [25]. They studied the contributing physical factors on the frequency and critical velocity of the pipes carrying fluid. In particular, the induced vibration due to fluid flow inside the rotating cantilever pipes raises a significant and challenging research topic because it is a critical issue in the design of the fluidic devices. Therefore, it is crucial to know the mechanical behavior of rotating pipes conveying fluid. In this regard, Panussis and Dimarogonas [26] examined the comparisons between in-plane and out-of-plane lateral vibrations and rotating effect on the critical flutter speed and frequency of a horizontally rotating cantilever pipe conveying fluid. Yoon and Son [27] analytically analyzed the influences of rotating angular velocity, tip mass and fluid velocity on the dynamic behavior of a cantilever pipe. Wang and Zhang [28] studied the dynamic behavior of a rotating pipe containing flowing fluid using the radial basis collocation method. Khajehpour and Azadi [29] investigated vibration analysis of a rotating cantilever pipe carrying fluid with piezoelectric layers and subjected to tip mass. The effects of rotating angular velocity, the fluid velocity and magnitude of uniformly distributed tangential follower force on the flutter instability of a rotating pipe conveying fluid were studied by Karimi-Nobandegani et al. [30]. Free vibration analysis of the rotating/spinning single-walled carbon nanotubes (SWCNTs) conveying fluid was analyzed by Safarpour and Ghadiri [31]. They obtained the influences of material length scale parameter, fluid velocity, angular velocity, aspect ratio and boundary conditions on the critical velocity and natural frequency. The above literature review shows that there is no research on the dynamics of the rotating cantilever pipes containing flowing flow for the FG-CNTRC beams.

The problems of vibration and structural stability in the thin-walled beams have been attracted numerous attentions in mechanical engineering, aerospace engineering, civil engineering, energy harvesting issues and many other applications. The studies of such problems are always of practical engineering interest, and consequently, an enormous amount of research work has been done in this field. Thermoelastic vibration and instability analysis of the rotating/spinning thin-walled beam made of functionally graded materials (FGMs) were studied by Librescu et al. [32]. They studied the effects of volume fraction, temperature gradient, compressive axial load and rotational/spinning speed on the vibration and instability of the system. The vibration and instability of the spinning thin-walled shafts made of FGMs and subjected to compressive axial load in thermal environment were investigated by Oh et al. [33]. The rotating FGM thin-walled beam under aerothermoelastic loading based on the Timoshenko beam theory was also studied [34,35]. The mechanical behavior of thin-walled structures has been studied by many researchers (see, e.g., Oh et al. [36], Sina et al. [37], Li et al. [38] and Cihan et al. [39]). The FG thin-walled Rayleigh beam model was developed by Hosseini and Fazelzadeh [40] to investigate the thermomechanical stability analysis of the cantilever pipes conveying fluid subjected to compressive axial load. Using thin-walled Rayleigh beam theory, Eftekhari and Hosseini [41] investigated the stability of the spinning pipes made of FGMs under compressive axial load. Choi et al. [42] studied the nonlinear vibration and instability behaviors of the nanopipes conveying fluid based on the thin-walled beam theory. Yun et al. [43] performed the fluid-induced vibration and flutter instability of a cantilever multi-walled carbon nanotube (MWCNT) subjected to axial flow. In their work, the nanotubes were modeled as thin-walled Euler–Bernoulli and Timoshenko beams.

The above literature review illustrations that there is no published research concerning the analysis of the critical flutter velocity of thin-walled FG-CNTRC rotating pipe conveying fluid. So, this manuscript is aimed to investigate the dynamic behavior of a thin-walled FG-CNTRC rotating pipe carrying fluid. Uniform and three

types of functionally graded distributions of CNTs along the thickness direction of the thin-walled rotating pipe are considered. To obtain the equivalent material properties of an FG-CNTRC pipe, the rule of mixture is utilized. Based on the thin-walled Timoshenko beam theory, the equations of motion are derived via Hamilton's principle and they are discretized by the extended Galerkin method. The resulting eigenvalue problem is then solved, and some numerical results are investigated to study the effects of length–radius ratio, nanotube volume fraction, CNT distribution, rotational speed and mass ratio on the dimensionless eigenfrequency and critical flutter velocity of the system.

2 The basic formulation

Figure 1 depicts the fluid-conveying thin-walled rotating pipe reinforced by FG-CNTs with length L, thickness h and middle cord radius r_m. The blade is mounted on a rigid hub of radius R_0 which is rotating about the axis of symmetry with constant angular velocity ω_0. The reference coordinates (x, y, z) are defined as local coordinates associated with the blade, and another coordinates (s, n, z) are used to define a complex cross-section profile.

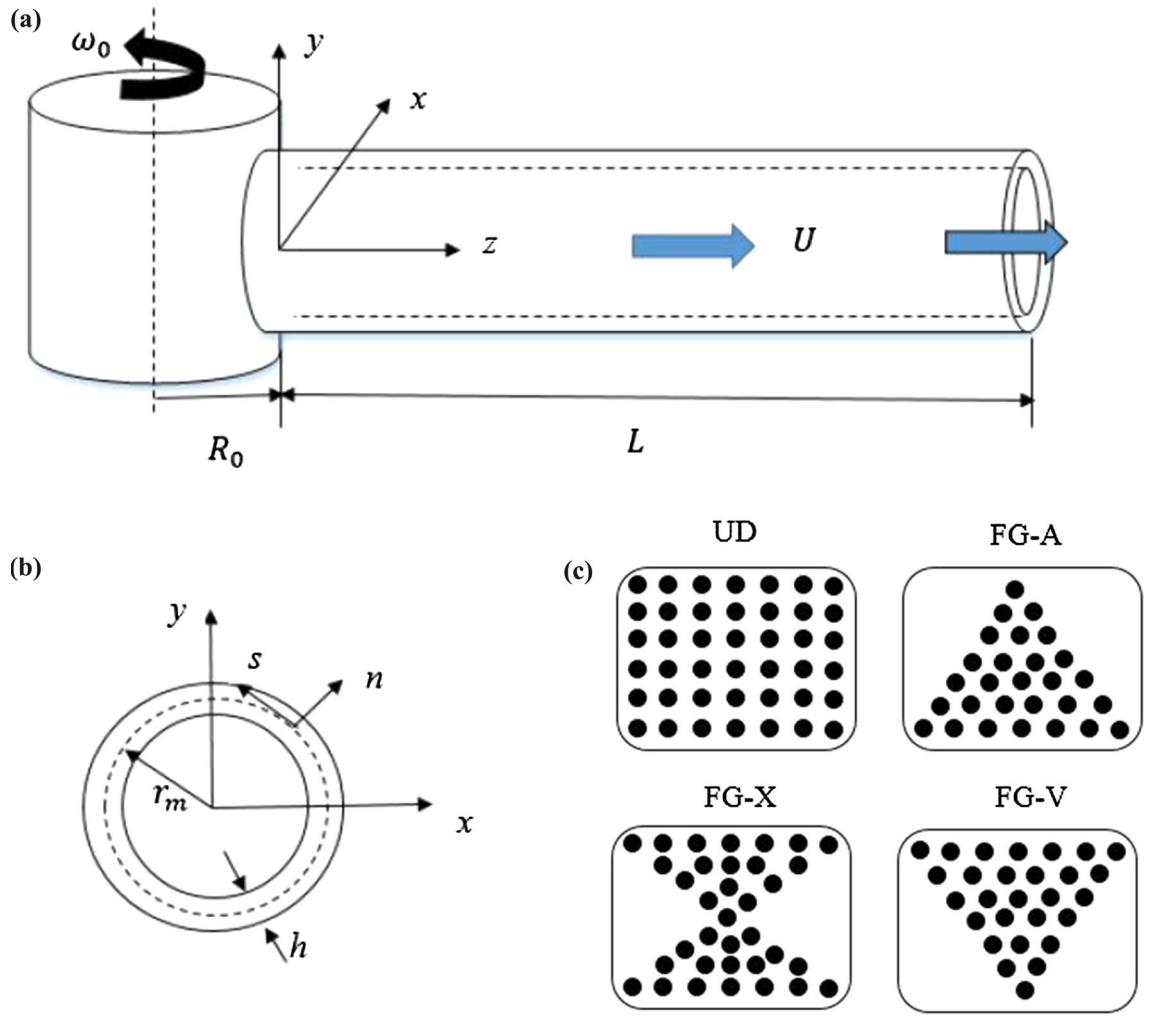

Fig. 1 Schematic diagram of a thin-walled CNTRC rotating pipe conveying fluid: **a** geometry and coordinate system, **b** the cross section of the pipe, **c** distribution types of CNTs

2.1 Kinematics

The displacements field of a thin-walled Timoshenko pipe can be expressed as [32]

$$\begin{aligned} u_1(x, y, z; t) &= u_0(z; t), \\ u_2(x, y, z; t) &= v_0(z; t), \\ u_3(x, y, z; t) &= w_0(z; t) + \theta_x(z; t)\left[y(s) - n\frac{\mathrm{d}x}{\mathrm{d}s}\right] + \theta_y(z; t)\left[x(s) + n\frac{\mathrm{d}y}{\mathrm{d}s}\right], \end{aligned} \tag{1}$$

where $u_0(z; t)$, $v_0(z; t)$ and $w_0(z; t)$ denote the rigid body translations along the x, y and z axes and $\theta_x(z; t)$ and $\theta_y(z; t)$ represent the rigid body rotations about the x and y axes, respectively. Furthermore, $x(s)$ and $y(s)$ denote the position of the circumferential centerline, while n denotes the outward directed distance from this centerline. The expressions for $\theta_x(z; t)$ and $\theta_y(z; t)$ can be written as [32]

$$\begin{aligned} \theta_x(z; t) &= \gamma_{yz}(z; t) - v_0'(z; t), \\ \theta_y(z; t) &= \gamma_{xz}(z; t) - u_0'(z; t), \end{aligned} \tag{2}$$

where γ_{yz} and γ_{xz} are the transverse shear strains.

The strain–displacement relationship can be written as

$$\varepsilon_{zz} = \frac{\partial u_3}{\partial z}, \quad \gamma_{xz} = \frac{\partial u_3}{\partial x} + \frac{\partial u_1}{\partial z}, \quad \gamma_{yz} = \frac{\partial u_3}{\partial y} + \frac{\partial u_2}{\partial z}, \quad \varepsilon_{xx} = \varepsilon_{yy} = \gamma_{xy} = 0. \tag{3}$$

The relation between strains in (s, z, n) and (x, y, z) coordinate systems can be obtained as

$$\varepsilon_{sz} = \frac{\mathrm{d}x}{\mathrm{d}s}\gamma_{xz} + \frac{\mathrm{d}y}{\mathrm{d}s}\gamma_{yz}, \quad \varepsilon_{nz} = \frac{\mathrm{d}y}{\mathrm{d}s}\gamma_{xz} - \frac{\mathrm{d}x}{\mathrm{d}s}\gamma_{yz}, \quad \varepsilon_{nn} = \varepsilon_{ss} = \varepsilon_{sn} = 0. \tag{4}$$

The position vector of an arbitrary point on the deformed pipe can be formulated as [32]

$$\boldsymbol{R}(x, y, z; t) = (x + u_1)\boldsymbol{i} + (y + u_2)\boldsymbol{j} + (z + u_3)\boldsymbol{k} + \boldsymbol{R}_0. \tag{5}$$

Furthermore, the velocity vector of an arbitrary point can be obtained by taking the time derivative of the position vector as

$$\dot{\boldsymbol{R}} = [\dot{u}_1 + (R_0 + z + u_3)\omega_0]\,\boldsymbol{i} + \dot{u}_2\boldsymbol{j} + [\dot{u}_3 - (x + u_1)\omega_0]\,\boldsymbol{k}, \tag{6}$$

where the superposed dots denote time derivatives. The fluid velocity particle is defined as

$$\boldsymbol{v}_f = \left[\dot{u}_1 + (R_0 + z + u_3)\,\omega_0 + U\frac{\partial u_0}{\partial z}\right]\boldsymbol{i} + \left[\dot{u}_2 + U\frac{\partial v_0}{\partial z}\right]\boldsymbol{j} + \left[\dot{u}_3 - (x + u_1)\,\omega_0 + y_f\dot{\theta}_x + x_f\dot{\theta}_y + U\right]\boldsymbol{k}. \tag{7}$$

Herein, the subscript f stands for the fluid.

2.2 Constitutive equations for FG-CNTRC pipes

The constitutive relations for the thin-walled FG-CNTRC Timoshenko pipes can be formulated as

$$\begin{bmatrix} \sigma_{ss} \\ \sigma_{zz} \\ \sigma_{zn} \\ \sigma_{sn} \\ \sigma_{zs} \end{bmatrix} = \begin{bmatrix} Q_{11} & Q_{12} & 0 & 0 & 0 \\ Q_{12} & Q_{22} & 0 & 0 & 0 \\ 0 & 0 & Q_{44} & 0 & 0 \\ 0 & 0 & 0 & Q_{55} & 0 \\ 0 & 0 & 0 & 0 & Q_{66} \end{bmatrix} \begin{bmatrix} \varepsilon_{ss} \\ \varepsilon_{zz} \\ \gamma_{zn} \\ \gamma_{sn} \\ \gamma_{zs} \end{bmatrix}, \tag{8}$$

where

$$\begin{aligned} Q_{11} &= \frac{E_{11}}{1 - \nu_{12}\nu_{21}}, \quad Q_{12} = \frac{\nu_{12}E_{22}}{1 - \nu_{12}\nu_{21}}, \quad Q_{22} = \frac{E_{22}}{1 - \nu_{12}\nu_{21}}, \\ Q_{44} &= Q_{55} = \kappa_s^2 G_{12}, \quad Q_{66} = G_{12}. \end{aligned} \tag{9}$$

In Eq. (9), $\kappa_s^2 = \pi^2/12$ is the transverse shear correction factor. Also, E_{11}, E_{22}, G_{12}, ν_{12} and ν_{21} denote the effective Young's and shear moduli and Poisson's ratios of the CNTRC pipe, respectively. The thin-walled pipe is a mixture of the CNTs, and a polymer matrix and the effective material properties may be written as [44]

$$\begin{aligned} E_{11} &= \eta_1 V^{\mathrm{CNT}} E_{11}^{\mathrm{CNT}} + V^m E^m, \\ \frac{\eta_2}{E_{22}} &= \frac{V^{\mathrm{CNT}}}{E_{22}^{\mathrm{CNT}}} + \frac{V^m}{E^m}, \\ \frac{\eta_3}{G_{12}} &= \frac{V^{\mathrm{CNT}}}{G_{12}^{\mathrm{CNT}}} + \frac{V^m}{G^m}, \end{aligned} \tag{10}$$

where E_{11}^{CNT}, E_{22}^{CNT} and G_{12}^{CNT} represent Young's and shear moduli of the CNTs, E^m and G^m denote the corresponding properties for polymer matrix and $\eta_i (i = 1, 2, 3)$ represent the CNT efficiency parameters, respectively. The values of the CNT efficiency parameters, the size dependency of material properties, can be determined by comparison of effective elastic moduli of CNTRC, resulting from the molecular dynamics procedure and the rule of mixture. Besides, V^{CNT} and V^m represent the volume fractions of the CNT and matrix, respectively, satisfying

$$V^{\mathrm{CNT}} + V^m = 1. \tag{11}$$

Four different distributions of CNTs along the thickness direction of the thin-walled pipes are assumed [5]:

$$UD : V^{\mathrm{CNT}}(z) = V_0^{\mathrm{CNT}}, \tag{12a}$$

$$FG - A : V^{\mathrm{CNT}}(z) = \left(1 - \frac{2n}{h}\right) V_0^{\mathrm{CNT}}, \quad h/2 \le n \le h/2, \tag{12b}$$

$$FG - V : V^{\mathrm{CNT}}(z) = \left(1 + \frac{2n}{h}\right) V_0^{\mathrm{CNT}}, \tag{12c}$$

$$FG - X : V^{\mathrm{CNT}}(z) = \frac{4|n|}{h} V_0^{\mathrm{CNT}}, \tag{12d}$$

where

$$V_0^{\mathrm{CNT}} = \frac{\omega^{\mathrm{CNT}}}{\omega^{\mathrm{CNT}} + (\rho^{\mathrm{CNT}}/\rho^m)(1 - \omega^{\mathrm{CNT}})}. \tag{13}$$

Also, ω^{CNT} denotes the mass fraction of CNT, and $\rho^{\mathrm{CNT}}$and ρ^m are the density of the CNT and matrix, respectively. Similarly, the mass density and Poisson's ratio can be determined as [5]

$$\rho = V^{\mathrm{CNT}} \rho^{\mathrm{CNT}} + V^m \rho^m, \tag{14}$$

$$\upsilon_{12} = V_0^{\mathrm{CNT}} \upsilon_{12}^{\mathrm{CNT}} + V^m \upsilon^m, \tag{15}$$

in which $\upsilon_{12}^{\mathrm{CNT}}$ and υ^m denote Poisson's ratios of the CNT and matrix, respectively.

2.3 Governing equations

The dynamical governing equations of the system can be derived via the extended Hamilton's principle that might be formulated as [13]

$$\begin{aligned} &\int_{t_1}^{t_2} \left(\delta T_p + \delta T_f - \delta E - MU\left(\dot{\boldsymbol{R}}_L + U\boldsymbol{\tau}_L\right).\delta \boldsymbol{R}_L\right) \mathrm{d}t = 0, \\ &\delta u_0 = \delta v_0 = \delta \theta_x = \delta \theta_y = 0 \text{ at } t = t_1, t_2, \end{aligned} \tag{16}$$

where δT_p, δT_f and δE represent the variational form of the pipe kinetic, fluid kinetic and strain energies, respectively. Also, $\boldsymbol{R}_L$ and $\boldsymbol{\tau}_L$ denote the position vector of a point on the free ended axis and the tangential vector to the free ended axis of the pipe, respectively.

The variation of the kinetic energy of the thin-walled Timoshenko rotating pipe conveying fluid flow can be given by

$$\begin{aligned}\int_{t_1}^{t_2} \delta T \, \mathrm{d}t &= \int_{t_1}^{t_2} \left(\delta T_p + \delta T_f\right) \mathrm{d}t \\ &= -\int_{t_1}^{t_2} \mathrm{d}t \int_{z_1}^{z_2} \oint_c \int_{-\frac{h}{2}}^{\frac{h}{2}} \rho \left(\ddot{\boldsymbol{R}}.\delta \boldsymbol{R}\right) \mathrm{d}n\mathrm{d}s\mathrm{d}z - \int_{t_1}^{t_2} dt \int_{z_1}^{z_2} M \left(\boldsymbol{v}_f.\delta \boldsymbol{v}_f\right) \mathrm{d}z. \end{aligned} \tag{17}$$

The variation of the strain energy based on the thin-walled Timoshenko beam theory is given by [32]

$$\delta E = \int_0^L \oint_c \int_{-\frac{h}{2}}^{\frac{h}{2}} \left(\sigma_{zz}\, \delta\varepsilon_{zz} + \sigma_{sz}\, \delta\gamma_{sz} + \sigma_{nz}\, \delta\gamma_{nz}\right) \mathrm{d}n\, \mathrm{d}s\, \mathrm{d}z. \tag{18}$$

Here, the following stress resultants are employed:

$$\begin{aligned} N_{zz} &= \int_{-\frac{h}{2}}^{\frac{h}{2}} \sigma_{zz}\, \mathrm{d}n, \quad L_{zz} = \int_{-\frac{h}{2}}^{\frac{h}{2}} \sigma_{zz}\, n\, \mathrm{d}n, \\ N_{sz} &= \int_{-\frac{h}{2}}^{\frac{h}{2}} \sigma_{sz}\, \mathrm{d}n, \quad N_{nz} = \int_{-\frac{h}{2}}^{\frac{h}{2}} \sigma_{nz}\, \mathrm{d}n. \end{aligned} \tag{19}$$

So, the variation of strain energy can be rewritten as

$$\begin{aligned}\delta E = \frac{1}{2}\int_{z_1}^{z_2} \oint_c \Bigg\{ & N_{zz}\, \delta \left[\frac{\partial w}{\partial z} + y\,(s)\,\frac{\partial \theta_x}{\partial z} + x\,(s)\,\frac{\partial \theta_y}{\partial z} + \frac{1}{2}\left(\left(\frac{\partial u_0}{\partial z}\right)^2 + \left(\frac{\partial v_0}{\partial z}\right)^2\right)\right] \\ & + L_{zz}\, \delta \left[\frac{\mathrm{d}y(s)}{\mathrm{d}s}\frac{\partial \theta_y}{\partial z} - \frac{\mathrm{d}x(s)}{\mathrm{d}s}\frac{\partial \theta_x}{\partial z}\right] + N_{sz}\, \delta \left[\left(\theta_y + \frac{\partial u_0}{\partial z}\right)\frac{\mathrm{d}x(s)}{\mathrm{d}s} + \left(\theta_x + \frac{\partial v_0}{\partial z}\right)\frac{\mathrm{d}y(s)}{\mathrm{d}s}\right] \\ & + N_{nz}\, \delta \left[\left(\theta_y + \frac{\partial u_0}{\partial z}\right)\frac{\mathrm{d}y(s)}{\mathrm{d}s} - \left(\theta_x + \frac{\partial v_0}{\partial z}\right)\frac{\mathrm{d}x(s)}{\mathrm{d}s}\right]\Bigg\}\, \mathrm{d}s\, \mathrm{d}z. \end{aligned} \tag{20}$$

The stress resultants and stress couples are defined as follows:

$$\begin{aligned} T_z\,(z;t) &= \oint_c N_{zz}\, \mathrm{d}s, \\ Q_x\,(z;t) &= \oint_c \left[N_{sz}\frac{\mathrm{d}x\,(s)}{\mathrm{d}s} + N_{nz}\frac{\mathrm{d}y\,(s)}{\mathrm{d}s}\right]\mathrm{d}s, \\ Q_y\,(z;t) &= \oint_c \left[N_{sz}\frac{\mathrm{d}y\,(s)}{\mathrm{d}s} - N_{nz}\frac{\mathrm{d}x\,(s)}{\mathrm{d}s}\right]\mathrm{d}s, \\ M_x\,(z;t) &= \oint_c \left[y\, N_{zz} - L_{zz}\frac{\mathrm{d}x\,(s)}{\mathrm{d}s}\right]\mathrm{d}s, \\ M_y\,(z;t) &= \oint_c \left[x\, N_{zz} + L_{zz}\frac{\mathrm{d}y\,(s)}{\mathrm{d}s}\right]\mathrm{d}s, \end{aligned} \tag{21}$$

where T_z corresponds to the axial force; Q_x and Q_y are associated with the shear forces in x and y directions, respectively; and M_x and M_y are the bending moments about the x and y directions, respectively. Using the

above stress resultants and stress couples, the variation of the strain energy is expressed as follows:

$$\begin{aligned}\delta E = -\int_{z_1}^{z_2} \Bigg\{ & \frac{\partial T_z(z;t)}{\partial z}\delta w_0 + \left(\frac{\partial M_x(z;t)}{\partial z} - Q_y\right)\delta\theta_x \\ & + \left(\frac{\partial M_y(z;t)}{\partial z} - Q_x\right)\delta\theta_y + \left(\frac{\partial Q_x}{\partial z} + \frac{\partial}{\partial z}\left(T_z\frac{\partial u_0}{\partial z}\right)\right)\delta u_0 \\ & + \left(\frac{\partial Q_y}{\partial z} + \frac{\partial}{\partial z}\left(T_z\frac{\partial v_0}{\partial z}\right)\right)\delta v_0 \Bigg\}\,\mathrm{d}z + \Big\{T_z\delta w_0 + M_x\,\delta\theta_x + M_y\,\delta\theta_y \\ & + \left[Q_x + T_z\frac{\partial u_0}{\partial z}\right]\delta u_0 + \left[Q_y + T_z\frac{\partial v_0}{\partial z}\right]\delta v_0\Big\}\Big|_0^L . \end{aligned} \tag{22}$$

By substituting the above energy functions into Eq. (16), and using the calculus of variations principles, the equations of motion are expressed as

$$\begin{aligned}
&\delta u_0 : \left[a_{44}\left(u_0' + \theta_y\right) + a_{45}\left(v_0' + \theta_x\right)\right]' - (b_1 + M)\ddot{u}_0 + (b_1 + M)\omega_0^2 u_0 + \omega_0^2\left[R(z)\,u_0'\right]' \\
&\quad -2MU\dot{u}_0' - MU^2 u_0'' - 2b_1\omega_0\dot{w}_0 = 0, && (23)\\
&\delta v_0 : \left[a_{55}\left(v_0' + \theta_x\right) + a_{45}\left(u_0' + \theta_y\right)\right]' - (b_1 + M)\ddot{v}_0 + \omega_0^2\left[R(z)\,v_0'\right]' - 2MU\dot{v}_0' - MU^2 v_0'' = 0, && (24)\\
&\delta w_0 : \left[a_{11}w_0'\right]' - b_1\ddot{w}_0 + 2b_1\omega_0\dot{u}_0 + b_1\omega_0^2(R_0 + z + w_0) = 0, && (25)\\
&\delta\theta_y : [a_{22}\theta_y' + a_{23}\theta_x']' - a_{44}\left(u_0' + \theta_y\right) - a_{45}\left(v_0' + \theta_x\right) - (b_5 + b_{15})\left(\ddot{\theta}_y - \omega_0^2\theta_y\right) \\
&\quad - (b_6 - b_{13})\left(\ddot{\theta}_x - \omega_0^2\theta_x\right) - Mr_x^2\left(\ddot{\theta}_y - \omega_0^2\theta_y\right) = 0, && (26)\\
&\delta\theta_x : [a_{33}\theta_x' + a_{32}\theta_y']' - a_{55}(v_0' + \theta_x) - a_{54}(u_0' + \theta_y) - (b_4 + b_{14})(\ddot{\theta}_x - \omega_0^2\theta_x) \\
&\quad - (b_6 - b_{13})\left(\ddot{\theta}_y - \omega_0^2\theta_y\right) - Mr_y^2\left(\ddot{\theta}_x - \omega_0^2\theta_x\right) = 0, && (27)
\end{aligned}$$

where r_x and r_y denote the internal gyration radius of the cross-sectional area of the pipe flow passage about the x and y axes, respectively. The stiffness coefficients a_{ij} and b_{ij} can be found in Librescu et al. [32], and the associated boundary conditions are expressed as:
at $z = 0$

$$u_0 = v_0 = w_0 = \theta_y = \theta_x = 0, \tag{28}$$

at $z = L$

$$\begin{aligned}
&\delta u_0 : a_{44}\left(u_0' + \theta_y\right) + a_{45}\left(v_0' + \theta_x\right) = 0, && (29)\\
&\delta v_0 : a_{55}\left(v_0' + \theta_x\right) + a_{45}\left(u_0' + \theta_y\right) = 0, && (30)\\
&\delta w_0 : a_{11}w_0' = 0, && (31)\\
&\delta\theta_y : a_{22}\theta_y' + a_{23}\theta_x' = 0, && (32)\\
&\delta\theta_x : a_{33}\theta_x' + a_{32}\theta_y' = 0. && (33)
\end{aligned}$$

In the governing equations, $R(z)$ is the centrifugal force, which is defined as [45]

$$R(z) = \left[R_0(L - z) + \frac{1}{2}(L^2 - z^2)\right]. \tag{34}$$

For a pipe with circular cross section, $a_{44} = a_{55}$, $a_{22} = a_{33}$, $b_5 = b_6$, $b_{13} = b_{15}$, $r_x = r_y$ and $a_{45} = a_{54} = 0$.

3 Solution procedure

3.1 Galerkin method

Galerkin's method is a technique for discretizing partial differential equations with infinite degrees of freedom into a set of second-order ordinary differential equations with finite degrees of freedom. To that end, the following expansions which are expanded in a series of modes are assumed for the dimensionless displacements of the cantilever thin-walled pipe:

$$u_0(z;t)=\sum_{j=1}^{N}U_j(z)\,q_u(t)\,,\quad v_0(z;t)=\sum_{j=1}^{N}V_j(z)\,q_v(t)\,,\quad w_0(z;t)=\sum_{j=1}^{N}W_j(z)\,q_w(t)\,,$$
$$\theta_x(z;t)=\sum_{j=1}^{N}\Theta_x(z)\,q_x(t),\quad \theta_y(z;t)=\sum_{j=1}^{N}\Theta_y(z)\,q_y(t), \tag{35}$$

where $\boldsymbol{q}_u$, $\boldsymbol{q}_v$, $\boldsymbol{q}_w$, $\boldsymbol{q}_x$ and $\boldsymbol{q}_y$ are time-dependent vectors of generalized coordinates and $\boldsymbol{U}$, $\boldsymbol{V}$, $\boldsymbol{W}$, $\boldsymbol{\Theta_x}$ and $\boldsymbol{\Theta_y}$ are dimensional vectors of trial functions that satisfy the appropriate boundary conditions. For a cantilever thin-walled pipe, the following expansions are assumed [13]:

$$U(z)=V(z)=\frac{1}{\Omega_j^2}\left(\Theta_y(z)\right)''',$$
$$\Theta_y(z)=\Theta_x(z)=\left(q_j\cosh\left(q_j\right)+\frac{q_j^3}{p_j^2}\cos\left(p_j\right)\right)\cosh\left(q_jz\right)-\left(q_j\sinh\left(q_j\right)+p_j\sin\left(p_j\right)\right)\sinh\left(q_jz\right)$$
$$-\left(q_j\cosh\left(q_j\right)+\frac{q_j^3}{p_j^2}\cos\left(p_j\right)\right)\cos\left(q_jz\right)-\frac{q_j^3}{p_j^3}\left(q_j\sinh\left(q_j\right)+p_j\sin\left(p_j\right)\right)\sin\left(q_jz\right),$$
$$W(z)=\sin\left((2j-1)\,\pi z\right),$$
$$2p_j^2=\frac{\Omega_j^2}{\left(\frac{a_{44}L^2}{a_{33R}}\right)}+\left(\frac{\Omega_j^4}{\left(\frac{a_{44}L^2}{a_{33R}}\right)^2}+4\Omega_j^2\right)^{1/2},\quad 2q_j^2=-\frac{\Omega_j^2}{\left(\frac{a_{44}L^2}{a_{33R}}\right)}+\left(\frac{\Omega_j^4}{\left(\frac{a_{44}L^2}{a_{33R}}\right)^2}+4\Omega_j^2\right)^{1/2}, \tag{36}$$

where Ω_j is the jth eigenvalue of the cantilever beam and subscript R shows the properties of pure polymer matrix pipe. Substituting Eq. (35) into the governing equations and multiplying both sides of the equations by trial functions together with integration over the whole region, the following discretized expressions for the equations of motion can be expressed:

$$\boldsymbol{M}\ddot{\boldsymbol{q}}(t)+\boldsymbol{C}\dot{\boldsymbol{q}}(t)+\boldsymbol{K}\boldsymbol{q}(t)=0, \tag{37}$$

where $\boldsymbol{q}=\left[\boldsymbol{q}_u^T\boldsymbol{q}_v^T\,\boldsymbol{q}_w^T\boldsymbol{q}_x^T\,\boldsymbol{q}_y^T\right]^T$ denote the overall vector of generalized coordinates and $\boldsymbol{M}$, $\boldsymbol{C}$ and $\boldsymbol{K}$ denote mass, damping and stiffness matrices of the system. The expressions for the matrices are formulated as

$$\boldsymbol{M}=\begin{bmatrix}\boldsymbol{M}_{uu}&\boldsymbol{M}_{uv}&\boldsymbol{M}_{uw}&\boldsymbol{M}_{uy}&\boldsymbol{M}_{ux}\\ \boldsymbol{M}_{vu}&\boldsymbol{M}_{vv}&\boldsymbol{M}_{vw}&\boldsymbol{M}_{vy}&\boldsymbol{M}_{vx}\\ \boldsymbol{M}_{wu}&\boldsymbol{M}_{wv}&\boldsymbol{M}_{ww}&\boldsymbol{M}_{wy}&\boldsymbol{M}_{wx}\\ \boldsymbol{M}_{yu}&\boldsymbol{M}_{yv}&\boldsymbol{M}_{yw}&\boldsymbol{M}_{yy}&\boldsymbol{M}_{yx}\\ \boldsymbol{M}_{xu}&\boldsymbol{M}_{xv}&\boldsymbol{M}_{xw}&\boldsymbol{M}_{xy}&\boldsymbol{M}_{xx}\end{bmatrix},\quad \boldsymbol{C}=\begin{bmatrix}\boldsymbol{C}_{uu}&\boldsymbol{C}_{uv}&\boldsymbol{C}_{uw}&\boldsymbol{C}_{uy}&\boldsymbol{C}_{ux}\\ \boldsymbol{C}_{vu}&\boldsymbol{C}_{vv}&\boldsymbol{C}_{vw}&\boldsymbol{C}_{vy}&\boldsymbol{C}_{vx}\\ \boldsymbol{C}_{wu}&\boldsymbol{C}_{wv}&\boldsymbol{C}_{ww}&\boldsymbol{C}_{wy}&\boldsymbol{C}_{wx}\\ \boldsymbol{C}_{yu}&\boldsymbol{C}_{yv}&\boldsymbol{C}_{yw}&\boldsymbol{C}_{yy}&\boldsymbol{C}_{yx}\\ \boldsymbol{C}_{xu}&\boldsymbol{C}_{xv}&\boldsymbol{C}_{xw}&\boldsymbol{C}_{xy}&\boldsymbol{C}_{xx}\end{bmatrix},$$
$$\boldsymbol{K}=\begin{bmatrix}\boldsymbol{K}_{uu}&\boldsymbol{K}_{uv}&\boldsymbol{K}_{uw}&\boldsymbol{K}_{uy}&\boldsymbol{K}_{ux}\\ \boldsymbol{K}_{vu}&\boldsymbol{K}_{vv}&\boldsymbol{K}_{vw}&\boldsymbol{K}_{vy}&\boldsymbol{K}_{vx}\\ \boldsymbol{K}_{wu}&\boldsymbol{K}_{wv}&\boldsymbol{K}_{ww}&\boldsymbol{K}_{wy}&\boldsymbol{K}_{wx}\\ \boldsymbol{K}_{yu}&\boldsymbol{K}_{yv}&\boldsymbol{K}_{yw}&\boldsymbol{K}_{yy}&\boldsymbol{K}_{yx}\\ \boldsymbol{K}_{xu}&\boldsymbol{K}_{xv}&\boldsymbol{K}_{xw}&\boldsymbol{K}_{xy}&\boldsymbol{K}_{xx}\end{bmatrix}, \tag{38}$$

where

$$\boldsymbol{M}_{uu} = (b_1 + M)\int_0^L UU^T \mathrm{d}z, \quad \boldsymbol{M}_{uv} = \boldsymbol{M}_{uw} = \boldsymbol{M}_{uy} = \boldsymbol{M}_{ux} = 0,$$

$$\boldsymbol{C}_{uu} = 2MU\int_0^L U^{'}U^T \mathrm{d}z, \quad \boldsymbol{C}_{uw} = 2b_1\omega_0\int_0^L UW^T \mathrm{d}z, \quad \boldsymbol{C}_{uv} = \boldsymbol{C}_{uy} = \boldsymbol{C}_{ux} = 0,$$

$$\boldsymbol{K}_{uu} = \int_0^L \left(a_{44} + R(z)\omega_0^2)U^{'}U^{'T} + MU^2U^{''}U^T - (b_1 + M)\,\omega_0^2 UU^T\right)\mathrm{d}z,$$

$$\boldsymbol{K}_{uv} = \boldsymbol{K}_{uw} = \boldsymbol{K}_{ux} = 0, \qquad \boldsymbol{K}_{uy} = a_{44}\int_0^L \Theta_y U^{'T}\mathrm{d}z,$$

$$\boldsymbol{M}_{vv} = (b_1 + M)\int_0^L VV^T \mathrm{d}z, \quad \boldsymbol{M}_{vu} = \boldsymbol{M}_{vw} = \boldsymbol{M}_{vy} = \boldsymbol{M}_{vx} = 0,$$

$$\boldsymbol{C}_{vv} = 2MU\int_0^L V^{'}V^T \mathrm{d}z, \qquad \boldsymbol{C}_{vu} = \boldsymbol{C}_{vw} = \boldsymbol{C}_{vy} = \boldsymbol{C}_{vx} = 0,$$

$$\boldsymbol{K}_{vv} = \int_0^L \left(a_{55} + R(z)\omega_0^2)V^{'}V^{'T} + MU^2V^{''}V^T\right)\mathrm{d}x,$$

$$\boldsymbol{K}_{vu} = \boldsymbol{K}_{vw} = \boldsymbol{K}_{vy} = 0, \quad \boldsymbol{K}_{vx} = a_{55}\int_0^L \Theta_x V^{'T}\mathrm{d}z,$$

$$\boldsymbol{M}_{wu} = \boldsymbol{M}_{wv} = \boldsymbol{M}_{wx} = \boldsymbol{M}_{wy} = 0, \qquad \boldsymbol{M}_{ww} = b_1\int_0^L WW^T \mathrm{d}z,$$

$$\boldsymbol{C}_{wv} = \boldsymbol{C}_{wx} = \boldsymbol{C}_{ww} = \boldsymbol{C}_{wy} = 0, \quad \boldsymbol{C}_{wu} = -2b_1\omega_0\int_0^L WU^T \mathrm{d}z$$

$$\boldsymbol{K}_{wu} = \boldsymbol{K}_{wv} = \boldsymbol{K}_{wy} = \boldsymbol{K}_{wx} = 0, \quad \boldsymbol{K}_{ww} = \int_0^L \left(a_{11}W^{'}W^{'T} - b_1\omega_0^2 WW^T\right)\mathrm{d}z,$$

$$\boldsymbol{M}_{yy} = \left(b_5 + b_{15} + Mr_x^2\right)\int_0^L \Theta_y\Theta_y^T \mathrm{d}z \quad \boldsymbol{M}_{yu} = \boldsymbol{M}_{yv} = \boldsymbol{M}_{yw} = 0,$$

$$\boldsymbol{M}_{yx} = (b_6 - b_{13})\int_0^L \Theta_x\Theta_y^T \mathrm{d}z,$$

$$\boldsymbol{C}_{yy} = \boldsymbol{C}_{yu} = \boldsymbol{C}_{yv} = \boldsymbol{C}_{yw} = \boldsymbol{C}_{yx} = 0,$$

$$\boldsymbol{K}_{yy} = \int_0^L \left(a_{22}\Theta_y^{'}\Theta_y^{'T} + (a_{44} - \omega_0^2(b_5 + b_{15} + Mr_x^2))\Theta_y\Theta_y^T\right)\mathrm{d}z,$$

$$\boldsymbol{K}_{yu} = a_{44}\int_0^L U^{'}\Theta_y^T \mathrm{d}z, \quad \boldsymbol{K}_{yv} = \boldsymbol{K}_{yw} = 0,$$

$$\boldsymbol{K}_{yx} = \int_0^L \left(a_{23}\Theta_x^{'}\Theta_y^{'T} - \omega_0^2\,(b_6 - b_{13})\,\Theta_x\Theta_y^T\right)\mathrm{d}x,$$

$$\boldsymbol{M}_{xx} = \left(b_4 + b_{14} + Mr_y^2\right)\int_0^L \Theta_x\Theta_x^T \mathrm{d}z, \quad \boldsymbol{M}_{xu} = \boldsymbol{M}_{xv} = \boldsymbol{M}_{xw} = 0,$$

$$\boldsymbol{M}_{xy} = (b_6 - b_{13})\int_0^L \Theta_y\Theta_x^T \mathrm{d}z,$$

$$\boldsymbol{C}_{xx} = \boldsymbol{C}_{xu} = \boldsymbol{C}_{xv} = \boldsymbol{C}_{xw} = \boldsymbol{C}_{xy} = 0,$$

$$\boldsymbol{K}_{xx} = \int_0^L \left(a_{33}\Theta_x^{'}\Theta_x^{'T} + (a_{55} - \omega_0^2(b_4 + b_{14} + Mr_y^2)\Theta_x\Theta_x^T\right)\mathrm{d}z,$$

$$\boldsymbol{K}_{xu} = \boldsymbol{K}_{xw} = 0, \quad \boldsymbol{K}_{xv} = a_{55}\int_0^L V^{'}\Theta_x^T \mathrm{d}z,$$

$$\boldsymbol{K}_{xy} = \int_0^L \left(a_{32} \Theta_y^{'} \Theta_x^{'T} - \omega_0^2 \left(b_6 - b_{13} \right) \Theta_y \Theta_x^T \right) \mathrm{d}z. \tag{39}$$

The matrix equation (37) can be transformed into a first-order state space form as

$$\dot{\boldsymbol{Z}}(t) = \boldsymbol{D}\boldsymbol{Z}(t), \tag{40}$$

where

$$\boldsymbol{Z}(t) = \begin{Bmatrix} q(t) \\ \dot{q}(t) \end{Bmatrix}, \quad \boldsymbol{D} = \begin{bmatrix} \boldsymbol{0} & \boldsymbol{I} \\ -\boldsymbol{M}^{-1}\boldsymbol{K} & -\boldsymbol{M}^{-1}\boldsymbol{C} \end{bmatrix}, \tag{41}$$

where $\boldsymbol{I}$ is the unitary matrix. Substituting the state vector $\boldsymbol{Z}(t) = \bar{\boldsymbol{Z}} \mathrm{e}^{(\Omega_0 i t)}$ into Eq. (40), the standard eigenvalue problem reads

$$(\boldsymbol{D} - i\Omega_0 \boldsymbol{I})\bar{\boldsymbol{Z}} = 0. \tag{42}$$

Generally, the eigenvalues Ω_0 are complex quantities, i.e., $\Omega_0 = Re(\Omega_0) + iIm(\Omega_0)$. Stability and type of instability regions can be defined based on the sign of the real and imaginary parts of the complex eigenvalues [46,47].

4 Results and discussion

Vibration and dynamic stability of the thin-walled CNTRC rotating fluid-conveying pipe with a circular cross section with the mean radius $r_m = 0.127\,\mathrm{m}$, uniform thickness $h = 0.1\,r_m$, length $L = 16\,r_m$ and hub radius $R_0 = 1.3\,\mathrm{m}$ are investigated [32]. The solution of this problem is obtained through the Galerkin method with six modes ($N = 6$). The CNTRC pipe is a mixture of CNTs and a polymer matrix. Poly{(m-phenylenevinylene)-co-[(2,5-dioctoxy-p-phenylene) vinyl-ene]}, PMPV, has been used as polymer matrix, and its material properties are: $E^m = 2.1\,\mathrm{GPa}$, $\rho^m = 1150\,\mathrm{kg/m^3}$ and $v^m = 0.34$ at room temperature [48]. Furthermore, the pipe is reinforced with single-walled CNTs whose material properties are taken to be $E_{11}^{\mathrm{CNT}} = 5.6466\,\mathrm{TPa}$, $E_{22}^{\mathrm{CNT}} = 7.0800\,\mathrm{TPa}$, $G_{12}^{\mathrm{CNT}} = 1.9445\,\mathrm{TPa}$, $v_{12}^{\mathrm{CNT}} = 0.175$, and $\rho^{\mathrm{CNT}} = 1400\,\mathrm{kg/m^3}$ [48]. In addition, the values of the efficiency parameters have been taken from those reported by Zhu et al. [48] as: $\eta_1 = 0.149$ and $\eta_2 = 0.934$ for $V_0^{\mathrm{CNT}} = 0.11$, $\eta_1 = 0.150$ and $\eta_2 = 0.941$ for $V_0^{\mathrm{CNT}} = 0.14$, moreover, $\eta_1 = 0.149$ and $\eta_2 = 1.381$ for $V_0^{\mathrm{CNT}} = 0.17$, and $\eta_3 = \eta_2$.

To simplify the analysis, the following dimensionless parameters are considered:

$$u = \sqrt{\frac{M}{a_{33R}}} UL, \quad \omega = \sqrt{\frac{(M + b_{1R})L^4}{a_{33R}}} \omega_0, \quad \beta = \frac{M}{M + b_{1R}}, \quad \Omega = \sqrt{\frac{(M + b_{1R})L^4}{a_{33R}}} \Omega_0.$$

A convergence study is implemented in Table 1 for the non-dimensional eigenfrequencies of cantilever thin-walled rotating pipe conveying fluid. The eigenvalue solution is performed for a thin-walled rotating pipe with FG-X distribution with $V_0^{\mathrm{CNT}} = 0.11$, $\beta = 0.5$, $u = 2$ and $\omega = 2$. The number of trial functions, N, was increased, and the eigenvalues were computed again. It is observed that the first three eigenvalues of the system do not change significantly at a sufficient number of trial functions. Increasing the number of trial functions further reduces the relative error but increases the computational time. Obviously, an optimum number of trial

Table 1 Convergence and accuracy of the first three eigenvalues for cantilever thin-walled pipe conveying fluid for various numbers of trial functions (N), (FG-X distribution, $\beta = 0.5$, $u = 2$, $\omega = 2$)

N			
3	$3.7544 + 1.9359i$	$19.2700 + 1.5013i$	$46.6238 + 1.7223i$
4	$3.7234 + 1.9302i$	$19.2110 + 1.4596i$	$43.9210 + 1.4164i$
5	$3.7266 + 1.9291i$	$19.0047 + 1.4370i$	$43.7568 + 1.3342i$
6	$3.7092 + 1.9221i$	$18.8954 + 1.4204i$	$43.3453 + 1.3082i$
7	$3.7065 + 1.9207i$	$18.8923 + 1.4202i$	$43.2812 + 1.2789i$
8	$3.7038 + 1.9205i$	$18.8914 + 1.4073i$	$43.0690 + 1.2769i$
9	$3.7003 + 1.9202i$	$18.8908 + 1.3979i$	$42.9964 + 1.2700i$

Table 2 Comparison of the present results with those reported in Ref. [43]

r_i/r_o^*	u_{cr}		Difference (%)
	Yun et al. [43]	Present study	
0.1	18.698	18.851	0.82
0.3	6.976	7.035	0.85
0.5	4.743	4.787	0.93
0.69	5.079	5.128	0.96
0.7	5.033	5.078	0.89
0.9	3.281	3.311	0.91

*Here r_i and r_o are inner and outer radius

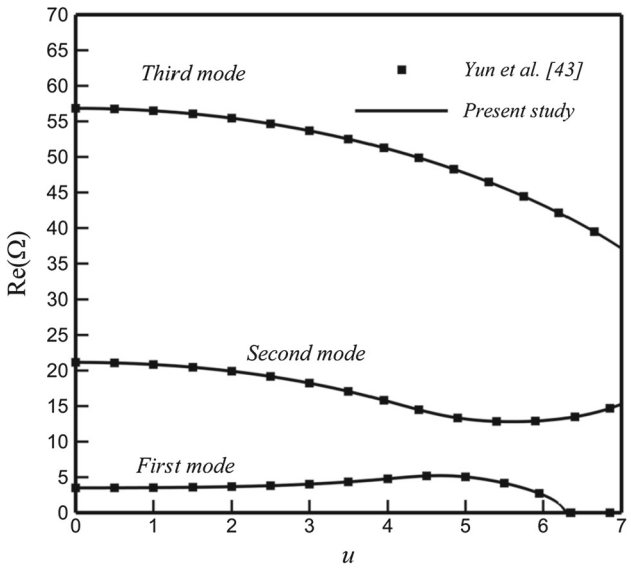

Fig. 2 The comparison between the results of current model and those reported by Yun et al. [43]

functions were chosen to reduce the computational time while achieving accurate results. We found that six trial functions can be used for achieving a solution with a relative error of less than 0.3% for the eigenfrequencies.

To investigate the validity and accuracy of the results, Table 2 and Fig. 2 show the comparisons of the dimensionless flutter velocity and dimensionless natural frequency for a thin-walled Timoshenko pipe conveying fluid. The properties of the materials considered in this validation are given as [43]: Young's moduli $E = 1\,\text{TPa}$; mass density $\rho_t = 2300\,\text{kg/m}^3$; length $L = 800\,\text{nm}$; outer radius $R_{\text{out}} = 40\,\text{nm}$; thickness $h = 20\,\text{nm}$; and Poisson's ratio $\upsilon = 0.25$. It is observed that the results of the present study are in good agreement with those of Yun et al. [43]. Furthermore, the figure shows that the fluid velocity considerably affects the first three natural frequencies and causes them to decrease.

Figure 3 illustrates the effects of different CNT distributions on the eigenfrequency of the three lowest modes of a cantilever thin-walled pipe conveying fluid as a function of the fluid velocity. The results are presented for $L = 10\,r_m$, $\beta = 0.5$, $V_0^{\text{CNT}} = 0.11$ and $\omega = 0$. It should be noted that the fluid velocity is known as the critical flutter velocity at which $Im(\Omega) = 0$ and $Re(\Omega) \neq 0$. Besides, the positive value of the imaginary part of the eigenfrequency reveals that the system is stable and the negative one is related to an unstable system. Also, when the sign of the imaginary part of the eigenfrequency changes from positive to negative, the flutter instability occurs. So, for small values of the fluid velocity as it is shown in Fig. 3a, all modes are stable since the flow induces positive damping in all modes, while for higher values of fluid velocity, the imaginary part of the third mode begins to decrease and eventually becomes negative at $u_{cr} = 6.145$. In other words, the cantilever rotating pipe loses its stability via a Hopf bifurcation which leads to the third-mode flutter. Furthermore, for fluid-conveying pipes reinforced by CNTs, the flutter may also occur in the second and third modes. The mode exchange is a frequently occurring feature of the dynamics of the system which has been detected in the FG-CNT pipes conveying fluid for the first time. From Fig. 3b, it is found that the flutter instability occurs in the third mode; therefore, the UD pipe loses its stability at lower critical flutter velocity

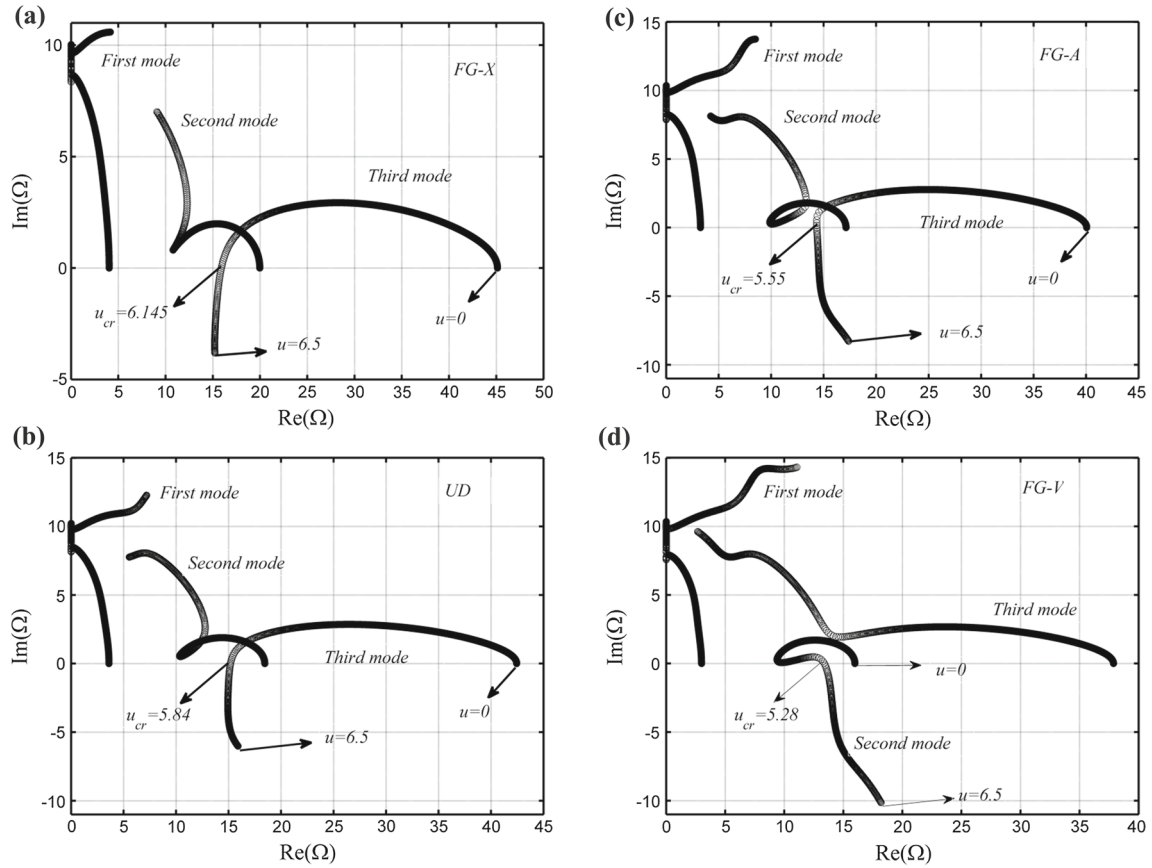

Fig. 3 The dimensionless complex eigenfrequency of the three lowest modes of the fluid-conveying thin-walled pipe as a function of u with $V_0^{\mathrm{CNT}} = 0.11$, $L = 10\,r_m$, $\beta = 0.5$ and $\omega = 0$, for different CNTs distribution types **a** FG-X, **b** UD, **c** FG-A, **d** FG-V

than the previous case (FG-X). For the FG-A type of CNT distribution, it can be observed from Fig. 3c that the critical fluid velocity occurs in the third mode at $u = u_{cr} = 5.55$. Furthermore, Fig. 3d shows that the fluid-conveying thin-walled pipe reinforced with FG-V type of CNTs distribution loses its stability via flutter in the second mode at $u_{cr} = 5.28$. Besides, it is seen that the flutter velocity predicted for the FG-X pipe is higher than that predicted for the other CNTRC distribution patterns.

Figure 4 is plotted to show the variations of the first three complex eigenfrequencies of the thin-walled rotating pipe conveying fluid versus the fluid velocity. The results of Fig. 4 are presented for the UD type of CNT distribution, $L = 10r_m$, $\beta = 0.5$, $V_0^{\mathrm{CNT}} = 0.11$ and various values of the rotational speed. The results indicated that by increasing the rotational speed, the critical flutter velocity increases. This means that the rise in the critical flutter velocity is due to additional restoring force of the centrifugal effect. Moreover, by the increase in the rotational speed, the mode-exchange phenomenon cannot be observed.

Figure 5 shows the variation of critical flutter velocity versus the mass ratio for a thin-walled pipe conveying fluid with FG-X type of CNT distribution, $V_0^{\mathrm{CNT}} = 0.11$ and $\omega = 0$. The curves in this figure, which separate the stable zone from the unstable, are called flutter boundaries. The flutter boundaries have several S-shaped sequences that represent different dynamic behaviors of the pipe conveying fluid, which has previously been detected by Gregory and Païdoussis [49]. This figure shows that the increase in the mass ratio leads to an increase in the critical fluid velocity. Also, the mode shapes change at the critical mass ratio [50]. In this figure, it is observed that the system remains stable when the fluid velocity is lower than the critical fluid velocity and any vibrational motions die out. Furthermore, the system becomes unstable and any perturbation will grow quickly at fluid velocity higher than the critical fluid velocity. Moreover, the length–radius ratio has a significant effect on the critical flutter velocity of thin-walled pipe conveying fluid. In other words, increasing the length–radius ratio increases the critical flutter velocity and the stable zone.

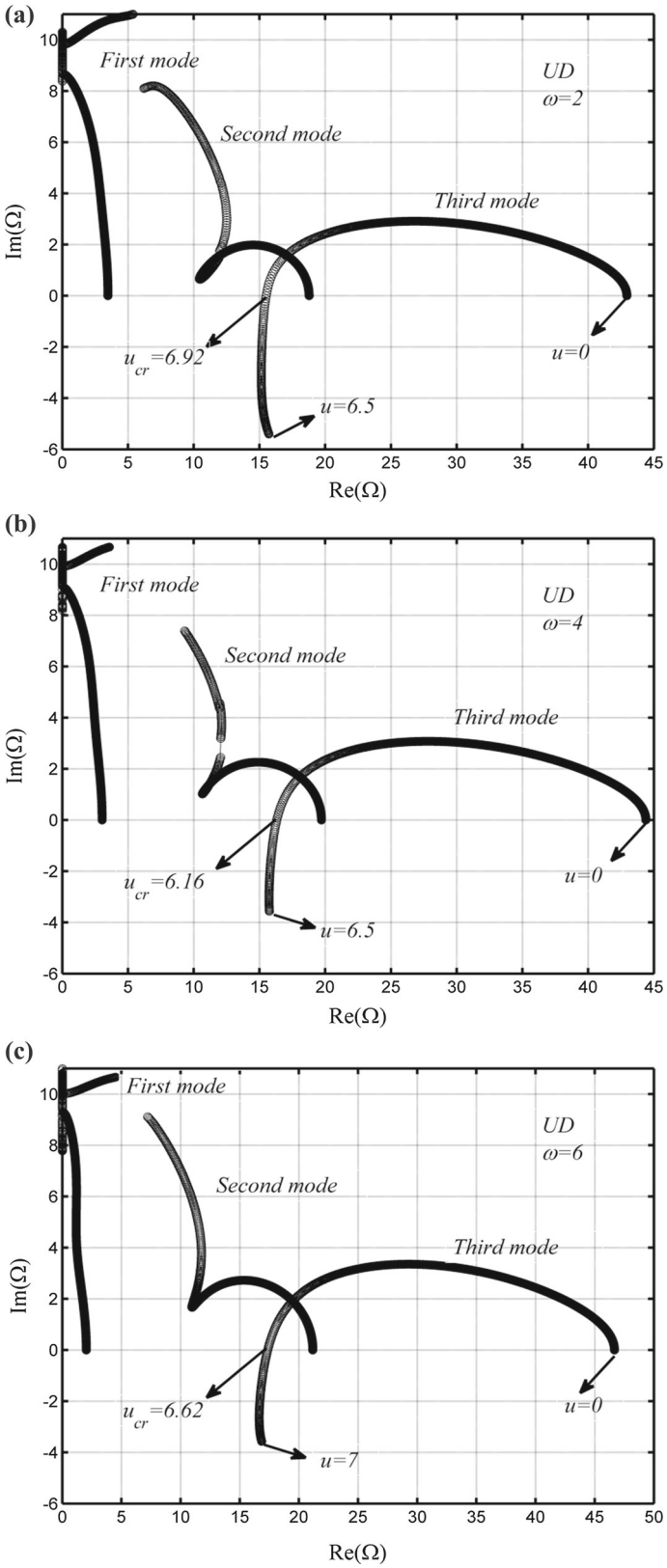

Fig. 4 The dimensionless complex eigenfrequency of the three lowest modes of the fluid-conveying thin-walled pipe as a function of u with $L = 10\,r_m$, UD distribution of CNTs, $V_0^{\mathrm{CNT}} = 0.11$, and $\beta = 0.5$, for different rotational speed **a** $\omega = 2$, **b** $\omega = 4$, **c** $\omega = 6$

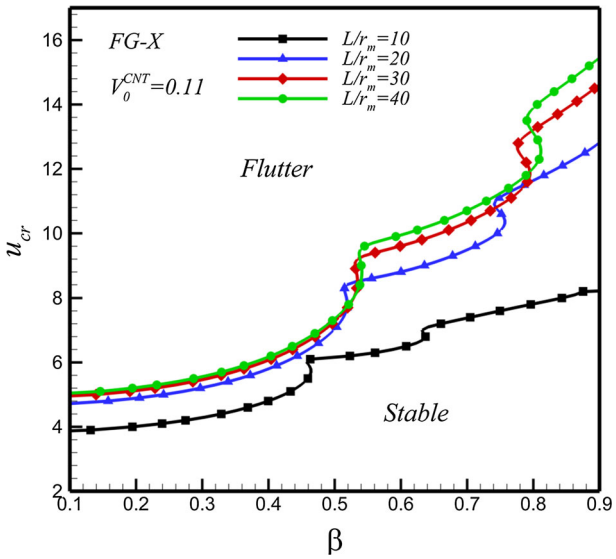

Fig. 5 Variation of the critical flutter velocity versus the mass ratio for a FG-X pipe with $\omega = 0$ and $V_0^{\mathrm{CNT}} = 0.11$, for different length–radius ratio

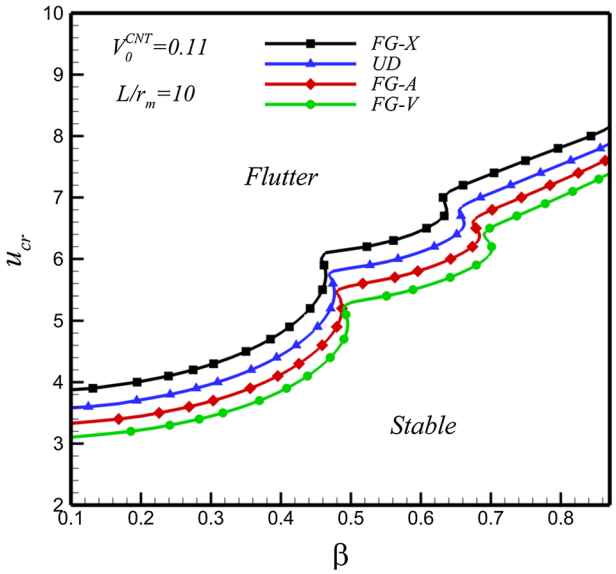

Fig. 6 Variation of the critical flutter velocity versus the mass ratio for various kinds of CNTRC pipe with $L = 10r_m$, $\omega = 0$ and $V_0^{\mathrm{CNT}} = 0.11$

To investigate the effects of various CNT distributions on the stability boundaries of the system, the critical flutter velocity versus the mass ratio is plotted in Fig. 6. The results are shown for $V_0^{\mathrm{CNT}} = 0.11$, $L = 10r_m$ and $\omega = 0$. It is clear that the stiffness of CNTRC pipes changes with the form of the CNT distribution in the matrix, and therefore, the distribution of CNTs considerably affects the stability zone of the system. It is observed that the FG-X pipe has the highest critical flutter velocity, whereas the FG-V pipe has the lowest critical flutter velocity among all distributions of CNTs. In other words, the results show that enhancing of the stiffness near the outer and inner surfaces of the pipe is an efficient way to improve the stability region.

It should be noted that the determination of critical fluid velocity and critical rotational speed of a thin-walled FG-CNTRC rotating pipe is of great importance. For this purpose, the variations of the critical flutter velocity by increasing the rotational speed for the different distributions of CNTs are plotted in Fig. 7. It is found that the critical flutter velocity increases when the rotational speed increases. Furthermore, the curves describe the relation between the critical flutter velocity and the critical rotational speed when the transference

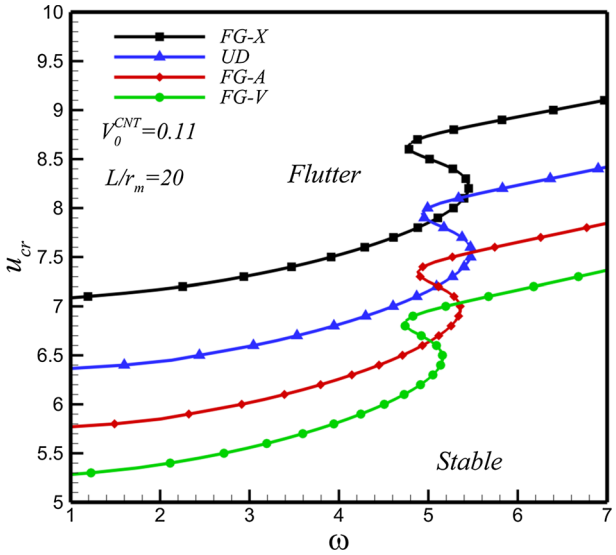

Fig. 7 Variation of the critical flutter velocity with the rotational speed for various kinds of CNTRC pipe with $L = 20r_m$, $\beta = 0.3$ and $V_0^{\mathrm{CNT}} = 0.11$

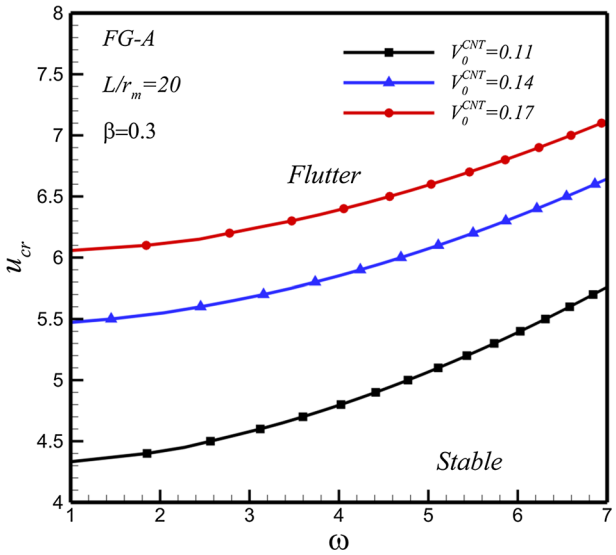

Fig. 8 Variation of the critical flutter velocity versus the rotational speed for a FG-A pipe with $L = 20r_m$ and $= 0.3$, for different V_0^{CNT}

of the two unstable modes occurs. It should be noted that the flutter instability of the FG-V pipe observed in the second and third modes in the range of $0 < \omega < 5.2$ and $5.2 < \omega < 7$, respectively, and the corresponding critical rotational speed is $\omega_{cr} \cong 5.2$. In addition, it is found that the CNT distribution close to both the inner and outer surfaces of the pipe (FG-X) is more effective than those distributed near the inner surface (FG-A) and outer surface (FG-V). This is due to the increase in the stiffness of the pipe.

The effect of the CNTs volume fraction on the flutter boundary of the FG-A pipe is plotted in Fig. 8. It is observed that by increasing the CNT volume fraction, the critical flutter velocity and stability region increase. In other words, the efficient approach to enhance the stability behaviors of a thin-walled pipe is to improve the structural stiffness and reduce the mass ratio.

5 Conclusion

Vibration and flutter instability of thin-walled FG-CNTRC rotating pipes conveying fluid were investigated in this study. Based on the thin-walled Timoshenko beam theory, the governing equations for vibration of the fluid-conveying rotating pipe were formulated by the use of Hamilton's principle. The extended Galerkin method was employed to discretize the governing equations, and the eigenfrequency and stability of the pipe were determined by eigenvalue analysis. To confirm the accuracy of the suggested model, the results were compared with the existing data in the literature. It was shown that by increasing both the length–radius ratio and mass ratio, the flutter velocity of the fluid-conveying thin-walled FG-CNTRC pipe increased. Also, the effectiveness of functionally graded distributions of CNTs in comparison with the uniform distribution of CNTs was investigated. Besides, by increasing the CNTs volume fraction, the critical flutter velocity of the pipe increased. Furthermore, the critical flutter velocity of the FG-X pipe was the maximum with respect to all CNT distribution patterns. In addition, the results indicated that the velocity of vibration-induced flutter instability of the thin-walled pipe increased as the rotational speed increased.

References

1. Bekyarova, E., Thostenson, E.T., Yu, A., Kim, H., Gao, J., Tang, J., Hahn, H.T., Chou, T.W., Itkis, M.E., Haddon, R.C.: Multiscale carbon nanotube-carbon fiber reinforcement for advanced epoxy composites. Langmuir **23**(5), 3970–3974 (2007)
2. Ke, L.L., Yang, J., Kitipornchai, S.: Nonlinear free vibration of functionally graded carbon nanotube-reinforced composite beams. Compos. Struct. **92**(3), 676–683 (2010)
3. Yas, M.H., Samadi, N.: Free vibrations and buckling analysis of carbon nanotube-reinforced composite Timoshenko beams on elastic foundation. Int. J. Press. Vessels Pip. **98**, 119–128 (2012)
4. Yas, M.H., Heshmati, M.: Dynamic analysis of functionally graded nanocomposite beams reinforced by randomly oriented carbon nanotube under the action of moving load. Appl. Math. Model. **36**(4), 1371–1394 (2012)
5. Rafiee, M., Yang, J., Kitipornchai, S.: Large amplitude vibration of carbon nanotube reinforced functionally graded composite beams with piezoelectric layers. Compos. Struct. **96**, 716–725 (2013)
6. Lin, F., Xiang, Y.: Vibration of carbon nanotube reinforced composite beams based on the first and third order beam theories. Appl. Math. Model. **38**(15–16), 3741–3754 (2014)
7. Wattanasakulpong, N., Ungbhakorn, V.: Analytical solutions for bending, buckling and vibration responses of carbon nanotube-reinforced composite beams resting on elastic foundation. Comput. Mater. Sci. **71**, 201–208 (2013)
8. Fazelzadeh, S.A., Pouresmaeeli, S., Ghavanloo, E.: Aeroelastic characteristics of functionally graded carbon nanotube-reinforced composite plates under a supersonic flow. Comput. Methods Appl. Mech. Eng. **285**, 714–729 (2015)
9. Asadi, H., Souri, M., Wang, Q.: A numerical study on flow-induced instabilities of supersonic FG-CNT reinforced composite flat panels in thermal environments. Compos. Struct. **171**, 113–125 (2017)
10. Alibeigloo, A., Liew, K.M.: Elasticity solution of free vibration and bending behavior of functionally graded carbon nanotube-reinforced composite beam with thin piezoelectric layers using differential quadrature method. Int. J. Appl. Mech. **07**(01), 1550002 (2015)
11. Mirzaei, M., Kiani, Y.: Nonlinear free vibration of temperature-dependent sandwich beams with carbon nanotube-reinforced face sheets. Acta Mech. **227**(5), 1869–1884 (2016)
12. Thomas, B., Roy, T.: Vibration analysis of functionally graded carbon nanotube-reinforced composite shell structures. Acta Mech. **227**(2), 581–599 (2016)
13. Païdoussis, M.P.: Fluid-Structure Interactions: Slender Structures and Axial Flow, vol. 1. Academic Press, New York (1998)
14. Kuiper, G.L., Metrikine, A.V., Battjes, J.A.: A new time-domain drag description and its influence on the dynamic behaviour of a cantilever pipe conveying fluid. J. Fluids Struct. **23**(3), 429–445 (2007)
15. Ghorbanpour Arani, A., Dashti, P., Amir, S., Yousefi, M.: Nonlinear vibration of coupled nano-and microstructures conveying fluid based on Timoshenko beam model under two-dimensional magnetic field. Acta Mech. **226**(8), 2729–2760 (2015)
16. Hosseini, M., Bahaadini, R.: Size dependent stability analysis of cantilever micro-pipes conveying fluid based on modified strain gradient theory. Int. J. Eng. Sci. **101**, 1–13 (2016)
17. Ning, W.B., Zhang, J.G., Chen, W.D.: Dynamics and stability of a functionally graded cylindrical thin shell containing swirling annular fluid flow including initial axial loads. Acta Mech. **227**(8), 2157–2170 (2016)
18. Kjolsing, E.J., Todd, M.D.: Damping of a fluid-conveying pipe surrounded by a viscous annulus fluid. J. Sound Vib. **394**, 575–592 (2017)
19. Wang, B., Deng, Z., Ouyang, H., Wang, Y.: Terahertz wave propagation in a fluid-conveying single-walled carbon nanotube with initial stress subjected to temperature and magnetic fields. Acta Mech. **226**(9), 3031–3043 (2015)
20. Bahaadini, R., Hosseini, M., Jamalpoor, A.: Nonlocal and surface effects on the flutter instability of cantilevered nanotubes conveying fluid subjected to follower forces. Physica B Condens. Matter **509**, 55–61 (2017)
21. Bahaadini, R., Saidi, A.R., Hosseini, M.: On dynamics of nanotubes conveying nanoflow. Int. J. Eng. Sci. **123**, 181–196 (2018)
22. Bahaadini, R., Hosseini, M., Jamali, B.: Flutter and divergence instability of supported piezoelectric nanotubes conveying fluid. Physica B Condens. Matter **529**, 57–65 (2018)
23. Hosseini, M., Bahaadini, R., Jamali, B.: Nonlocal instability of cantilever piezoelectric carbon nanotubes by considering surface effects subjected to axial flow. J. Vib. Control **24**(9), 1809–1825 (2016)
24. Hosseini, M., Maryam, A.Z.B., Bahaadini, R.: Forced vibrations of fluid-conveyed double piezoelectric functionally graded micropipes subjected to moving load. Microfluid. Nanofluid. **21**(8), 134 (2017)

25. Askarian, A.R., Haddadpour, H., Firouz-Abadi, R.D., Abtahi, H.: Nonlinear dynamics of extensible viscoelastic cantilevered pipes conveying pulsatile flow with an end nozzle. Int. J. Non-Linear Mech. **91**, 22–35 (2017)
26. Panussis, D.A., Dimarogonas, A.D.: Linear in-plane and out-of-plane lateral vibrations of a horizontally rotating fluid-tube cantilever. J. Fluids Struct. **14**(1), 1–24 (2000)
27. Yoon, H.I., Son, I.S.: Dynamic response of rotating flexible cantilever pipe conveying fluid with tip mass. Int. J. Mech. Sci. **49**(5), 878–887 (2007)
28. Wang, L., Zhong, Z.: Radial basis collocation method for the dynamics of rotating flexible tube conveying fluid. Int. J. Appl. Mech. **7**(03), 1550045 (2015)
29. Khajehpour, S., Azadi, V.: Vibration suppression of a rotating flexible cantilever pipe conveying fluid using piezoelectric layers. Latin Am. J. Solids Struct. **12**(4), 1042–1060 (2015)
30. Karimi-Nobandegani, A., Fazelzadeh, S.A., Ghavanloo, E.: Effect of uniformly distributed tangential follower force on the stability of rotating cantilever tube conveying fluid. Latin Am. J. Solids Struct. **13**(2), 365–377 (2016)
31. Safarpour, H., Ghadiri, M.: Critical rotational speed, critical velocity of fluid flow and free vibration analysis of a spinning SWCNT conveying viscous fluid. Microfluid. Nanofluid. **21**(2), 22 (2017)
32. Librescu, L., Oh, S.Y., Song, O.: Thin-walled beams made of functionally graded materials and operating in a high temperature environment: vibration and stability. J. Therm. Stresses **28**(6–7), 649–712 (2005)
33. Oh, S.Y., Librescu, L., Song, O.: Vibration and instability of functionally graded circular cylindrical spinning thin-walled beams. J. Sound Vib. **285**(4), 1071–1091 (2005)
34. Fazelzadeh, S.A., Hosseini, M.: Aerothermoelastic behavior of supersonic rotating thin-walled beams made of functionally graded materials. J. Fluids Struct. **23**(8), 1251–1264 (2007)
35. Fazelzadeh, S.A., Malekzadeh, P., Zahedinejad, P., Hosseini, M.: Vibration analysis of functionally graded thin-walled rotating blades under high temperature supersonic flow using the differential quadrature method. J. Sound Vib. **306**(1), 333–348 (2007)
36. Oh, S.Y., Librescu, L., Song, O.: Vibration of turbomachinery rotating blades made-up of functionally graded materials and operating in a high temperature field. Acta Mech. **166**(1), 69–87 (2003)
37. Sina, S.A., Haddadpour, H., Navazi, H.M.: Nonlinear free vibrations of thin-walled beams in torsion. Acta Mech. **223**(6), 2135–2151 (2012)
38. Li, X., Li, Y.H., Qin, Y.: Free vibration characteristics of a spinning composite thin-walled beam under hygrothermal environment. Int. J. Mech. Sci. **119**, 253–265 (2016)
39. Cihan, M., Eken, S., Kaya, M.O.: Dynamic instability of spinning launch vehicles modeled as thin-walled composite beams. Acta Mech. **228**(12), 4353–4367 (2017)
40. Hosseini, M., Fazelzadeh, S.A.: Thermomechanical stability analysis of functionally graded thin-walled cantilever pipe with flowing fluid subjected to axial load. Int. J. Struct. Stab. Dyn. **11**(03), 513–534 (2011)
41. Eftekhari, M., Hosseini, M.: On the stability of spinning functionally graded cantilevered pipes subjected to fluid-thermomechanical loading. Int. J. Struct. Stab. Dyn. **16**(09), 1550062 (2015)
42. Choi, J., Song, O., Kim, S.K.: Nonlinear stability characteristics of carbon nanotubes conveying fluids. Acta Mech. **224**(5), 1383–1396 (2013)
43. Yun, K., Choi, J., Kim, S.K., Song, O.: Flow-induced vibration and stability analysis of multi-wall carbon nanotubes. J. Mech. Sci. Technol. **26**(12), 3911–3920 (2012)
44. Shen, H.S.: Nonlinear bending of functionally graded carbon nanotube-reinforced composite plates in thermal environments. Compos. Struct. **91**(1), 9–19 (2009)
45. Song, O., Librescu, L.: Structural modeling and free vibration analysis of rotating composite thin-walled beams. J. Am. Helicopter Soc. **42**(4), 358–369 (1997)
46. Bahaadini, R., Hosseini, M.: Effects of nonlocal elasticity and slip condition on vibration and stability analysis of viscoelastic cantilever carbon nanotubes conveying fluid. Comput. Mater. Sci. **114**, 151–159 (2016)
47. Bahaadini, R., Hosseini, M.: Flow-induced and mechanical stability of cantilever carbon nanotubes subjected to an axial compressive load. Appl. Math. Model. **59**, 597–613 (2018)
48. Zhu, P., Lei, Z.X., Liew, K.M.: Static and free vibration analyses of carbon nanotube-reinforced composite plates using finite element method with first order shear deformation plate theory. Compos. Struct. **94**(4), 1450–1460 (2012)
49. Gregory, R.W., Païdoussis, M.P.: Unstable oscillation of tubular cantilevers conveying fluid. I. Theory. Proc. R. Soc. Lond. A Math. Phys. Eng. Sci. **1435**, 512–527 (1966)
50. Bahaadini, R., Hosseini, M.: Nonlocal divergence and flutter instability analysis of embedded fluid-conveying carbon nanotube under magnetic field. Microfluid. Nanofluid. **20**(5), 1–14 (2016)